



## Spectral description of oceanic near-surface variability

Shane Elipot<sup>1</sup> and Rick Lumpkin<sup>1</sup>

Received 6 December 2007; revised 22 January 2008; accepted 4 February 2008; published 7 March 2008.

[1] This paper provides a spectral description of near-surface oceanic velocity variability on a global scale. Rotary spectra of drifter velocities are estimated in zonal bands of the Indian, Pacific and Atlantic Oceans. The partition of energy between cyclonic and anticyclonic frequencies clearly identifies inertial oscillations at all latitudes. The meridional distribution of near-inertial energy is described in detail. The polarization of super-inertial energy is consistent with internal waves dynamics. Thus, the distribution of super-inertial energy may be a manifestation of freely propagating near-inertial waves on the  $\beta$ -plane. **Citation:** Elipot, S., and R. Lumpkin (2008), Spectral description of oceanic near-surface variability, *Geophys. Res. Lett.*, 35, L05606, doi:10.1029/2007GL032874.

### 1. Introduction

[2] Frequency spectra are used to study oceanic variability because their shape is expected to be dictated by the underlying dynamics. Oceanic variability spans a wide frequency range. As such, spectra have been investigated at low and mesoscale frequencies [Stammer, 1997; Zang and Wunsch, 2001; Lumpkin and Flament, 2001], at high and super-inertial frequencies [Garrett and Munk, 1979], and in specific frequency bands such as inertial and tidal, notably with the help of surface drifter velocity data [Crawford et al., 1998; Poulain et al., 1992].

[3] This study uses a high temporal resolution data set of positions of satellite-tracked surface drifters in which the latitudinal distribution of inertial, diurnal and semi-diurnal energy of near-surface oceanic velocities in the Indian, Pacific and Atlantic sectors of the World Ocean are accurately resolved. The characteristics of the variability at different time scales are investigated by analyzing velocity rotary spectra, and notably by estimating their polarization, which is a measure of the partition of energy between anticyclonic and cyclonic motions. Particular attention is directed to the near-inertial band, for which energy is estimated as a function of latitude in all three ocean sectors. The near-inertial and super inertial bands are of great importance for ocean energetics; mapping their energies should help in understanding their production and dissipation in the World Ocean.

### 2. Data and Methods

[4] The Global Drifter Program (<http://www.aoml.noaa.gov/phod/dac/gdp.html>) maintains a global array of satellite-tracked surface drifters which are drogued to follow currents at a nominal depth of 15 m. In recent years, the time interval between two consecutive position fixes of a drifter has de-

creased because, first, the 1-day-on-2-day off duty cycle for data transmission has been abandoned since 2000, and second, starting January 2005 the satellite tracking switched from a service of two satellites to between five and six satellites. As a consequence, the time interval between consecutive drifter position fixes now averages between 1 and 2 hours. Thus, information about motions at much higher frequencies than previously available is accessible in oceanic velocity time series derived from a drifter's displacement with time.

[5] From the quality controlled data set [Lumpkin and Pazos, 2007] spanning January 2000 to June 2007, we selected for this study the subset of drifter trajectories for which the drogue is retained and for which no time interval between two consecutive fixes was greater than 6 hours. Next, we interpolated the drifter positions using a spline scheme to regular hourly intervals. Time series of drifter velocities were then computed by a 2-hour centered difference.

[6] In order to achieve a compromise between data availability and spectral resolution we sorted the trajectories of hourly drifter position into  $2.5^\circ$  latitude bands in each oceanic sector: Indian, Pacific and Atlantic. The longitude dividing the Indian and Pacific sectors in the Southern Ocean is arbitrary. Coastal areas were also discarded (see Figure 1). For each band, we rejected drifter trajectory segments that ventured outside the band for more than 6 days, or began/ended more than 2.5 days outside the band.

[7] For each zonal band we identified continuous 40-day trajectory segments, overlapping by 20 days in order to increase the number of degrees of freedom. Shorter subsegments were rejected. From all the hourly velocity 40-day time series in each zonal band, a single rotary spectrum estimate was computed by the ensemble average periodogram method [Bendat and Piersol, 1986], applying a Hanning window to reduce spectral leakage (see Figure S1 of auxiliary material<sup>1</sup> for an example in one band). The resulting frequency bandwidth due to the time series length and the windowing [Harris, 1978] is 0.0375 cycles per day (cpd), and the Nyquist frequency is theoretically 6 cpd.

[8] Each satellite fix is associated with a quality index ranging from 3 (<150 m uncertainty) to 0 (>1000 m). If one assumes that this position noise has a white spectrum, then the velocity noise spectrum is a quadratic function of frequency [Rupolo et al., 1996]. Taking into account the different sampling intervals of the raw data set, and also examining the results a posteriori, we estimated the velocity noise level to be larger than any oceanic signal for frequencies greater than 4 cpd.

### 3. Results

#### 3.1. Rotary Spectra

[9] Rotary spectral analysis decomposes vector motions in counter-rotating circular components, which is particu-

<sup>1</sup>PhOD, AOML, NOAA, Miami, Florida, USA.

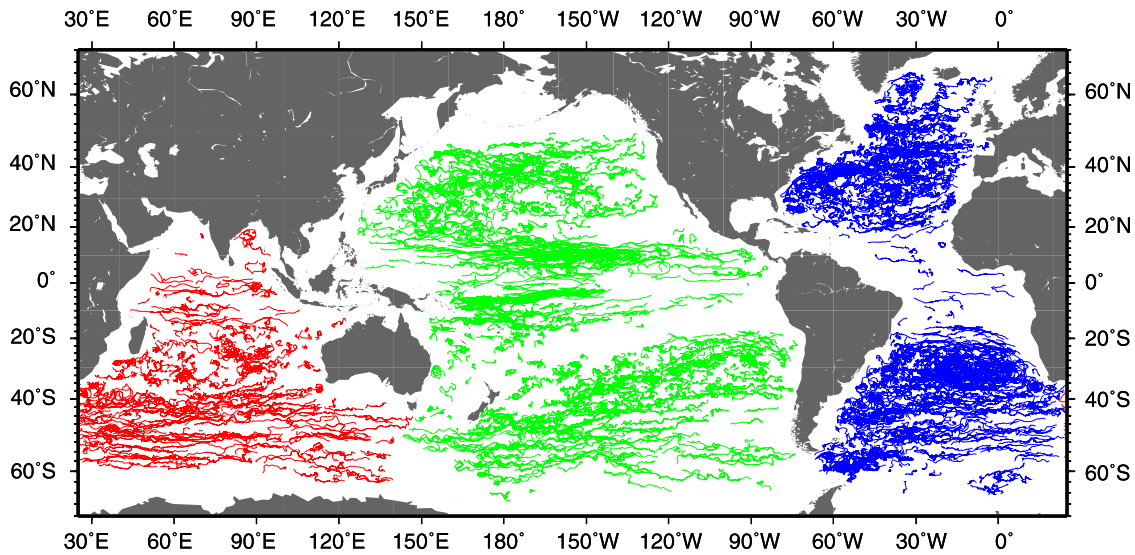


**Figure 1.** Drifter trajectory segments used for this study.

larly revealing for the study of geophysical flows influenced by Earth’s rotation [Gonella, 1972]. Counterclockwise motions (at positive frequencies) are cyclonic in the Northern Hemisphere, and anticyclonic in the Southern Hemisphere; the opposite is true for clockwise motions (negative frequencies).

[10] Figure 2 shows the velocity spectra for the Pacific Ocean. It is similar to the spectra in the Indian and Atlantic Oceans. The general characteristics of these frequency-latitude spectra are:

[11] 1. a “red” character in the cyclonic frequency domain, and also in the anticyclonic domain between frequency  $\nu = 0$  and approximately the local inertial frequency  $\nu = -f/(2\pi)$  in cpd, where  $f$  is the Coriolis parameter;

[12] 2. low frequency bands ( $|\nu| < 1/14$  cpd) dominated by the geostrophic component of the drifter velocities as confirmed by a cross-spectral analysis (see Figure S2 of auxiliary material) with geostrophic velocities estimated independently from altimetry data from AVISO [1996];

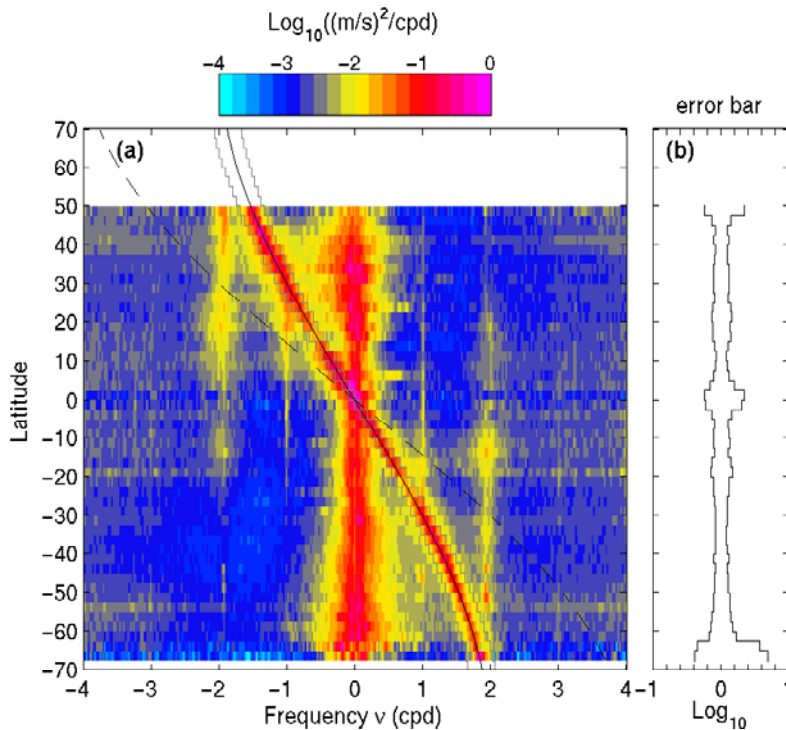


**Figure 2.** (a) Drifter velocity rotary power spectra in 2.5 degrees latitudinal bands in the Pacific Ocean. The continuous (dashed) line is (twice) the local inertial frequency; the gray lines are 90% (110%) of the minimum (maximum) inertial frequency of a given latitudinal band. (b) Error bars (no units) as a function of latitude: the 95% confidence interval for the true spectra  $S$  is written as a function of the spectral estimate  $\hat{S}$  as  $\alpha\hat{S} < S < \beta\hat{S}$ ; The left curve is  $\log_{10}(\alpha)$  and the right curve is  $\log_{10}(\beta)$ . These two curves are scaled to correspond to the colorbar for the rotary spectra.

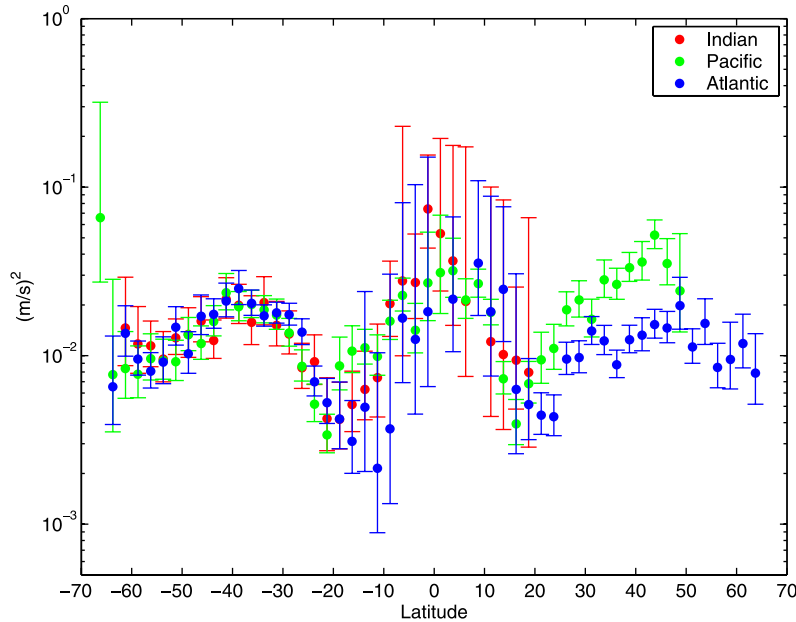


**Figure 3.** Drifter velocity variance in the near-inertial band for the Indian, Pacific and Atlantic basins in 2.5 degrees latitudinal bands. Error bars are derived from the 95% confidence intervals of the rotary spectrum estimates.

[13] 3. a prominent inertial peak of narrow width closely following  $\nu = -f/(2\pi)$ , almost as great as the zero frequency peak, with latitudinal variations (see also section 3.2);

[14] 4. broad peaks at  $\nu \approx \pm 2$  cpd for counter-clockwise (clockwise) frequencies between the most southern (northern) latitude and 20°N (S) likely ascribable to semidiurnal tidal forcing;

[15] 5. diurnal peaks in both frequency domains, noticeable predominantly from the latitude where the diurnal frequency is inertial (30°), spreading equatorward and ultimately continuing to the same latitude in the other hemisphere.

### 3.2. Near-Inertial Variance

[16] Figure 3 shows the near-inertial variance for each ocean. This was computed in each latitudinal band by integrating the spectra between 0.9 times the minimum inertial frequency in this band and 1.1 times the maximum inertial frequency, corresponding to the two gray lines in Figure 2a. The error bars are derived by computing the integral of the upper and lower estimates of the spectra in this frequency range. The main results are:

[17] 1. south of 30°S the inertial variance is statistically the same in each sector;

[18] 2. as mentioned previously, there is a dramatic reduction of the inertial variance by an order of magnitude from 45° to 15° in all sectors and both hemispheres; this was previously noted in the Northern Hemisphere by *Park et al.* [2005] who analyzed the surface drift of Argo floats;

[19] 3. in the Atlantic and Pacific Oceans, there is an asymmetry (albeit not significant) in the inertial variance as it increases by an order of magnitude across the equator from approximately 10°S to 10°N;

[20] 4. the overall largest variances (with the largest uncertainties) are found in the latitudinal bands on both sides of the Equator in the Indian Ocean and a few degrees

north in the Pacific and Atlantic Oceans, where the inertial band merges with the energetic low-frequency band;

[21] 5. the inertial variance is significantly higher in the Northern Pacific than in the Northern Atlantic from approximately 20°N to 50°N, also noticed by *Park et al.* [2005] who attributed this to different meridional patterns of mixed-layer depth and wind momentum input in each basin.

## 4. Characteristics of the Variability

### 4.1. Rotary Spectra Polarization

[22] The polarization of the spectrum can be a tool to help identify the processes causing the observed variability. *Gonella* [1972] defines a rotary coefficient  $r$  as

$$r = \frac{S^- - S^+}{S^- + S^+}, \quad (1)$$

where  $S^-$  ( $S^+$ ) is the clockwise (counterclockwise) spectrum, and as such the rotary coefficient is defined only for absolute frequencies. Here, the Southern Hemisphere convention is used for the sign of  $r$ . If  $r = 1$  ( $-1$ ) the motions in the given frequency band are purely cyclonic (anticyclonic) and circular; if  $r = 0$  the motions are rectilinear oscillating back and forth.

[23] The polarizations of the spectra in the Pacific, Atlantic and Indian Oceans are found to be very similar; Figure 4a shows the rotary coefficient for the Pacific. Only the statistically significant values are displayed, based on the 95% confidence interval of the rotary spectra. The general characteristics are:

[24] 1. a few occurrences of cyclonic polarization for  $|\nu| < 0.5$  cpd which could either be associated with mesoscale geostrophic motions (demonstrated by coherence estimation with geostrophic velocities) or possibly sub-mesoscale motions associated with frontal instabilities [*Griffa et al.*,

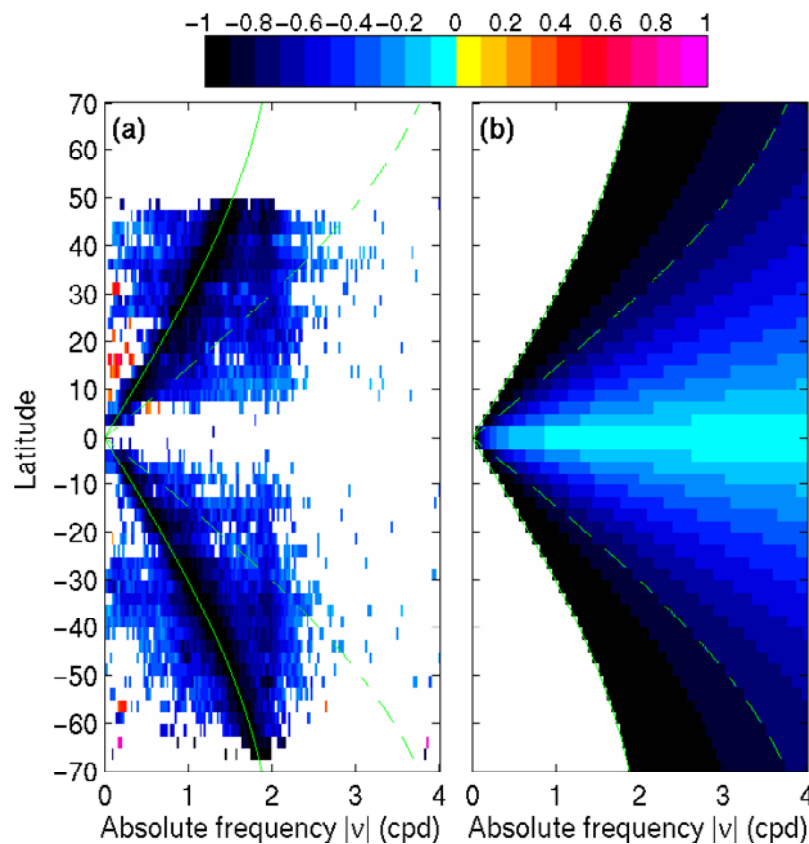


**Figure 4.** (a) Polarization of the rotary spectrum in the Pacific Ocean; only the statistically significant values are displayed. The continuous (dashed) green line is (twice) the local inertial frequency. (b) Theoretical polarization  $(-2 (2\pi|\nu|)|f|)/((2\pi\nu)^2 + f^2)$  for  $|\nu| \geq |f|/(2\pi)$ .

2008]; a drifter sampling bias towards region of cyclonic convergence may also explain these features [Middleton and Garrett, 1986];

[25] 2. purely anticyclonic polarization at  $|\nu| = |f|/(2\pi)$  cpd, showing the ubiquity of circular inertial oscillations at all latitudes, except in the two zonal bands just north and south of the Equator where data density is insufficient (also the case in the other oceans);

[26] 3. anticyclonic polarization at semi-diurnal frequency more pronounced than in neighboring frequency bands, most noticeable in the Atlantic (not shown);

[27] 4. a broad and dominantly anticyclonic polarization at sub-inertial frequencies between approximately  $20^\circ$  and  $50^\circ$  in both hemispheres which can be readily explained by frequency-dependent extensions of Ekman theory that predict a stronger anticyclonic response of locally forced Ekman currents to wind stress forcing [Gonella, 1972; Rio and Hernandez, 2003; Elipot, 2006];

[28] 5. for super-inertial frequencies, at a given latitude there is a general decrease of anticyclonic polarization with increasing frequencies; and at a constant frequency (except semi-diurnal) there is a general decrease of anticyclonic polarization with decreasing latitude from the latitude where this frequency is inertial, in both hemispheres.

#### 4.2. Discussion

[29] The velocity of a drifter along its trajectory is a result of various processes that contribute to its variance in overlapping,

yet discernible frequency bands. The current analyses suggest these processes to be predominantly geostrophic currents at low frequency domains, Ekman currents at sub-inertial frequencies, forced or free inertial oscillations at the inertial frequency, likely tidal oscillations at diurnal and semi-diurnal frequencies, and either directly wind-forced motion or freely propagating waves at super-inertial frequencies.

[30] What is the nature of the variance at super-inertial frequencies? To examine this further, the historical kriged 6-hourly drifter data set [Lumpkin and Pazos, 2007] was investigated jointly with 6-hourly wind stress reanalyses: the coherence between the drifter velocity and the wind stress drops significantly for frequencies above the inertial frequency. The 6-hourly data sets' lack of variance at high frequency may explain the super-inertial coherence drop at high latitudes but not at low latitudes. Using an explicit parametrization of the vertical viscosity in the context of Ekman dynamics, Elipot [2006] showed that the transfer function from the wind stress to Ekman velocity can explain the drop in coherence at high frequency. This being considered, the remaining variance of the spectrum at super-inertial frequencies is still to be explained.

[31] Is the spectrum at super-inertial frequencies compatible with inertia-gravity wave dynamics? To test this hypothesis we compare the observed rotary coefficient to theoretical predictions [e.g., Calman, 1978]. If the equation governing the evolution of the horizontal velocity  $\mathbf{u} = u + iv$

( $u$  and  $v$  are the zonal and meridional components;  $i$  is complex coefficient) is:

$$\frac{\partial \mathbf{u}}{\partial t} + i f \mathbf{u} = \mathbf{F}, \quad (2)$$

where  $\mathbf{F}$  is a forcing function with a spectrum which rotary coefficient is  $r_{\mathbf{F}}$ , then it can be shown that:

$$r_{\mathbf{u}}(|\nu|) = \frac{r_{\mathbf{F}} + g}{r_{\mathbf{F}}g + 1}, \quad \text{where} \quad g = \frac{-2(2\pi|\nu|)|f|}{(2\pi\nu)^2 + f^2}. \quad (3)$$

[32] For an internal wave background field, the “forcing” is the pressure perturbation field. If this is isotropic, then it has a white, and thus not polarized, spectrum so that  $r_{\mathbf{F}} = 0$  and  $r_{\mathbf{u}} = g$ , which is only a function of frequency [Fofonoff, 1969]. This law would also be applicable for near-inertial waves propagating in a two-layer model of the ocean [Gill, 1982].

[33] The theoretical law  $r_{\mathbf{u}} = g$  is plotted in Figure 4b for  $|\nu| > |f|/(2\pi)$ , the frequency domain in which oscillating waves can exist and propagate. There is some qualitative agreement which suggests indeed that the super-inertial variability is dominated by internal waves, generated locally or remotely. Moreover, the general confinement of anticyclonic polarization between the inertial latitude-frequency curve (green curve in Figure 4) and the Equator, most clear equatorward of  $25^\circ$  N or S, is consistent with the dispersion of internal waves on the  $\beta$ -plane: having been generated near their inertial latitude, internal waves are free to propagate between their critical latitudes (close to the inertial latitudes) in both hemispheres [Anderson and Gill, 1979]. This could corroborate localized observations at moorings [Alford, 2003].

[34] Discrepancies from the theoretical law could be due to many reasons: horizontally inhomogeneous forcing, dissipation and downward propagation, which means that the internal wave field is not isotropic, non linear interactions with transfers of energy between frequency bands, and of course other sources of variability. A detailed analysis of the variability at inertial and super-inertial frequencies is underway.

#### 4.3. Diurnal Variance

[35] Another striking characteristic is a “ridge” of enhanced energy at the diurnal frequency between  $30^\circ$  N and  $30^\circ$  S that might not be solely explained by tidal forcing. Other potential sources are inertial oscillations forced by the land-sea breeze [Gille et al., 2005] and subsequent propagation, or parametric sub-harmonic instability of the semi-diurnal barotropic tide that is only possible equatorwards of  $28.9^\circ$  [MacKinnon and Winters, 2005]. This is a subject requiring further and careful consideration.

#### 4.4. Epilogue

[36] Presently, the high temporal resolution data coverage is not sufficient to examine longitudinal variations of the spectra within the basins, which would be of interest for example to study the influence of bathymetry, notably at super-inertial frequencies. For this, drifter deployment efforts need to be sustained. However, the present analysis of near-surface variance should provide new benchmarks

for validating numerical models and testing dynamical hypothesis for oceanic variability, especially at near-inertial frequency.

[37] **Acknowledgments.** This research was performed while Shane Elipot held a National Research Council Research Associateship award at the Atlantic Oceanographic and Meteorological Laboratory (AOML). Rick Lumpkin was supported by NOAA’s Office of Climate Observations and AOML. The authors would like to thank Mayra Pazos, Jessica Redman and Erik Valdez of the GDP Data Assembly Center, who prepared the quality-controlled data set. The findings and conclusions in this report are those of the authors and do not represent necessarily the views of the funding agencies.

#### References

- Alford, M. (2003), Redistribution of energy available for ocean mixing by long-range propagation of internal waves, *Nature*, 423(6936), 159–162.
- Anderson, D., and A. Gill (1979), Beta dispersion of inertial waves, *J. Geophys. Res.*, 84(C4), 1836–1842.
- AVISO (1996), AVISO User Handbook for Merged TOPEX/POSEIDON Products, *AVI-NT-02-101-CN*, 3rd ed., Ramonville-Saint-Agne, France.
- Bendat, J. S., and A. G. Piersol (1986), *Random Data: Analysis and Measurement Procedures*, 3rd ed., 566 pp., John Wiley, Hoboken, N. J.
- Calman, J. (1978), On the interpretation of ocean current spectra, part II: Testing dynamical hypotheses, *J. Phys. Oceanogr.*, 8(4), 644–652.
- Crawford, W. R., J. Y. Chemiaowsky, and M. G. G. Foreman (1998), Rotary velocity spectra from short drifter tracks, *J. Atmos. Oceanic Technol.*, 15(3), 731–740.
- Elipot, S. (2006), Spectral characterization of Ekman velocities in the Southern Ocean based on surface drifter trajectories, Ph.D. thesis, Scripps Inst. of Oceanogr., Univ. of Calif., San Diego.
- Fofonoff, N. P. (1969), Spectral characteristics of internal waves in the ocean, *Deep Sea Res.*, 16, suppl., 58–71.
- Garrett, C., and W. Munk (1979), Internal waves in the ocean, *Annu. Rev. Fluid Mech.*, 11, 339–369.
- Gill, A. E. (1982), *Atmosphere-Ocean Dynamics*, 662 pp., Elsevier, New York.
- Gille, S. T., S. G. Llewellyn Smith, and N. M. Stom (2005), Global observations of the land breeze, *Geophys. Res. Lett.*, 32, L05605, doi:10.1029/2004GL022139.
- Gonella, J. (1972), A rotary-component method for analysing meteorological and oceanographic vector time series, *Deep Sea Res.*, 19, 833–846.
- Griffa, A., R. Lumpkin, and M. Veneziani (2008), Cyclonic and anticyclonic motion in the upper ocean, *Geophys. Res. Lett.*, 35, L01608, doi:10.1029/2007GL032100.
- Harris, F. J. (1978), On the use of windows for harmonic analysis with the discrete Fourier transform, *Proc. IEEE*, 66(1), 51–83.
- Lumpkin, R., and P. Flament (2001), Lagrangian statistics in the central North Pacific, *J. Mar. Syst.*, 29, 141–155.
- Lumpkin, R., and M. Pazos (2007), Measuring surface currents with SVP drifters: The instrument, its data, and some recent results, in *Lagrangian Analysis and Prediction of Coastal and Ocean Dynamics*, edited by A. Griffa et al., pp. 39–67, Cambridge Univ. Press, New York.
- MacKinnon, J., and K. Winters (2005), Subtropical catastrophe: Significant loss of low-mode tidal energy at  $28.9^\circ$ , *Geophys. Res. Lett.*, 32, L15605, doi:10.1029/2005GL023376.
- Middleton, J. F., and C. Garrett (1986), A kinematic analysis of polarized eddy fields using drifter data, *J. Geophys. Res.*, 91(C4), 5094–5102.
- Park, J., K. Kim, and B. A. King (2005), Global statistics of inertial motions, *Geophys. Res. Lett.*, 32, L14612, doi:10.1029/2005GL023258.
- Poulain, P.-M., D. S. Luther, and W. C. Patzert (1992), Deriving inertial wave characteristics from surface drifter velocities: Frequency variability in the tropical Pacific, *J. Geophys. Res.*, 97(C11), 17,947–17,959.
- Rio, M.-H., and F. Hernandez (2003), High-frequency response of wind-driven currents measured by drifting buoys and altimetry over the world ocean, *J. Geophys. Res.*, 108(C8), 3283, doi:10.1029/2002JC001655.
- Rupolo, V., L. H. Bach, A. Provenzale, and V. Artale (1996), Lagrangian velocity spectra at 700 m in the western North Atlantic, *J. Phys. Oceanogr.*, 26(8), 1591–1607.
- Stammer, D. (1997), Global characteristics of ocean variability estimated from regional TOPEX/POSEIDON altimeter measurements, *J. Phys. Oceanogr.*, 27(8), 1743–1769.
- Zang, X., and C. Wunsch (2001), Spectral description of low-frequency oceanic variability, *J. Phys. Oceanogr.*, 31(10), 3073–3095.

S. Elipot and R. Lumpkin, PhOD, AOML, NOAA, 4301 Rickenbacker Causeway, Miami, FL 33149, USA. (shane.elipot@noaa.gov)